Spatially heterogeneous wastage of Himalayan glaciers

Koji Fujita[1] **and Takayuki Nuimura**

Graduate School of Environmental Studies, Nagoya University, Chikusa-ku, Nagoya 464-8601, Japan

Edited by James E. Hansen, Goddard Institute for Space Studies, New York, NY, and approved June 29, 2011 (received for review April 19, 2011)

We describe volumetric changes in three benchmark glaciers in the Nepal Himalayas on which observations have been made since the 1970s. Compared with the global mean of glacier mass balance, the Himalayan glaciers showed rapid wastage in the 1970s–1990s, but similar wastage in the last decade. In the last decade, a glacier in an arid climate showed negative but suppressed mass balance compared with the period 1970s–1990s, whereas two glaciers in a humid climate showed accelerated wastage. A mass balance model with downscaled gridded datasets depicts the fate of the observed glaciers. We also show a spatially heterogeneous distribution of glacier wastage in the Asian highlands, even under the present-day climate warming.

climate change | equilibrium line altitude

A recent study (1) has highlighted gross inadequacies both in our knowledge of important changes occurring to Himalayan glaciers and in two recent reports that have alternately overestimated (2) and seriously underestimated (3) the pace of shrinkage of Himalayan glaciers without, in either report (2, 3), offering a compelling basis. However, the rate at which Himalayan glaciers are shrinking remains poorly constrained because ground-based measurements are hampered by the high altitude and remoteness of the region. This lack of observational data has given rise to large uncertainties in both observation-based (4–6) and simulation-based (7–9) projections of global sea-level rise. These studies relied on relationships established for well-studied glaciers under a Euro-American climate. However, this approach may be inaccurate because the seasonal cycle of precipitation has a strong effect on the surface albedo and thus on glacier melt in the monsoonal Asian region (10).

In addition, much of the debate on the fate of Himalayan glaciers has missed an important consideration of the height and trend of the equilibrium-line altitude (ELA), which divides the glacier into areas of ablation and accumulation (11). The ELA is important because, for example, if the glacier has no accumulation area for a period because the ELA is located above the glacier, the glacier is destined to disappear over time (12). Unfortunately, observations of the mass balance and ELA of Himalayan glaciers have been made only in recent years (13, 14).

To address these problems, in the present study we update the elevation data for Himalayan benchmark glaciers, providing information for the past decades. We calculate changes in the mass balance and ELA of the three benchmark glaciers using an energy-mass balance model with downscaled gridded climate datasets, in order to describe the state and fate of glaciers. Further calculations are performed to assess the spatial representativeness of the observation-based results.

Locations and Method

The three benchmark glaciers [Rikha Samba (RS), Yala (YL), and AX010 (AX)] are situated at diverse locations in the Nepal Himalayas (Fig. 1*A*). Changes in the surface elevation of these glaciers have been observed intermittently by geodetic surveys between the 1970s and the 1990s (14–17) (Figs. S1–S3). In this study, we conducted carrier-phase global positioning system (GPS) surveys between 2008 and 2010 to provide up-to-date data on changes in the elevations of the glacier surfaces since the most recent previous measurements in the 1990s (Figs. S4 and S5).

Results

Changes in Glacier Volume. Fig. 1*B* shows area-averaged mass balances (mass balance averaged for the entire glacier) calculated in this study along with those reported previously (14–17). Glacier wastage (negative mass balance) for the last decade is highly variable and is comparable to the global mean (6), whereas wastage in the previous two decades is much larger than the global mean. The RS glacier, in a comparatively arid area of western Nepal, shows suppressed wastage in the last decade compared with the previous two decades. In contrast, the two glaciers in a comparatively humid area of eastern Nepal show strongly accelerated wastage in the last decade.

A comparison of the mass balance results and annual precipitation reveals that glacier wastage has been accelerated in humid environments but suppressed in an arid environment (Fig. 1*C*). Previous observational (4, 16) and numerical (7, 10) studies have reported that glaciers respond more sensitively to warming in a humid environment in terms of mass balance. Glaciers in such an environment can exist at lower altitudes due to the large amount of snow accumulation, making them more sensitive to warming via changes in the fraction of precipitation occurring as rainfall (which affects accumulation) and changes in surface albedo (which affects ablation) (7, 10). Because the YL and AX glaciers are located in relatively humid environments and at lower altitudes (Fig. 1, Fig. S4, and Table S1), they are expected to show large amounts of wastage in response to recent warming.

Fate of Glaciers. To describe the fate of the three glaciers, we calculated their mass balance and ELA using an energy-mass balance model (18), employing recently archived gridded climate datasets (19, 20). We downscaled daily air temperature and precipitation in the datasets with those observed close to the glaciers for short periods (Table S2). Further calibration for air temperature was performed to yield the minimum rms error (rmse) against the surveyed area-averaged mass balance.

Fig. 2 shows the area–altitude distribution, calculated ELA, and preferable ELA for the present glacier extent (Fig. 2 *A*–*C*) and the calculated and surveyed area-averaged mass balance for each glacier (Fig. 2 *D*–*F*). Also shown are mass balances reconstructed from analyses of ice cores recovered from the RS and YL glaciers (21, 22). The preferable ELA is defined as the ELA in the case that its mass balance profile gives an area-averaged mass balance of zero; i.e., the glacier would retain its present extent if the ELA is located at the preferable altitude. All of the calculated

Author contributions: K.F. designed research; K.F. and T.N. performed research; K.F. and T.N. analyzed data; and K.F. wrote the paper.

The authors declare no conflict of interest.

This article is a PNAS Direct Submission.

Freely available online through the PNAS open access option.

[1]To whom correspondence should be addressed. E-mail: cozy@nagoya-u.jp.

This article contains supporting information online at www.pnas.org/lookup/suppl/doi:10.1073/pnas.1106242108/-/DCSupplemental.

ENVIRONMENTAL SCIENCES

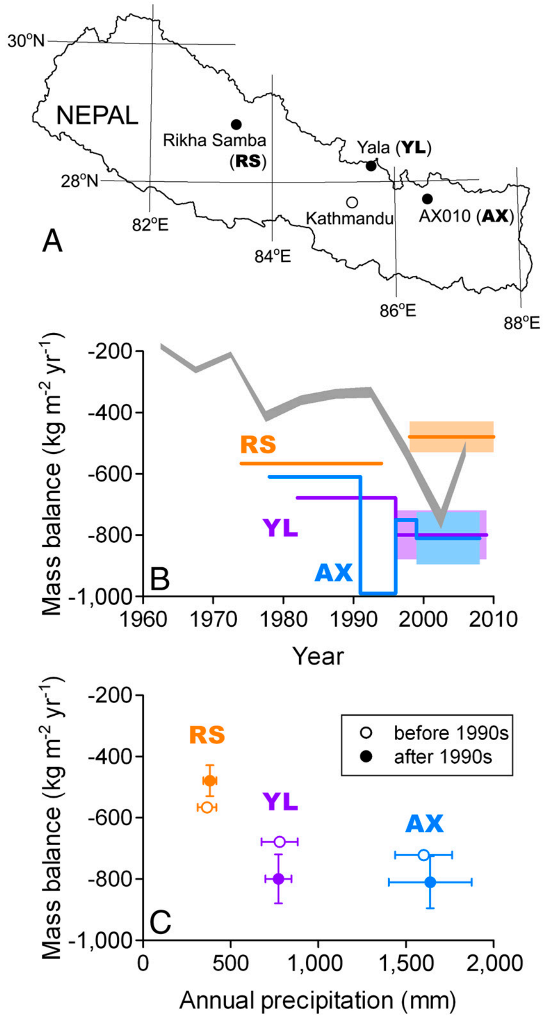

Fig. 1. Location of the three benchmark glaciers in Nepal (*A*), temporal changes in the area-averaged mass balances of the glaciers compared with the pentadal global mean (gray line) (6) (*B*), and mass balances compared with annual precipitation (*C*). Color shading in *B* and vertical bars in *C* denote measurement errors of mass balance. Horizontal bars in *C* denote variability of annual precipitation. See *SI Text* about the error evaluation and the downscaling.

ELAs are located above the preferable ELAs (Fig. 2 *A*–*C*); consequently, the area-averaged mass balances are all negative (except for the AX glacier in the 1970s and around 1990). However, the ELA for the RS glacier has fluctuated within the altitudinal extent of glacier and has descended since the 1990s, indicating that the glacier wastage has been suppressed in the last decade. If the present climate conditions persist, the RS glacier will approach an alternative equilibrium and will be maintained. In contrast, the ELAs of the YL and AX glaciers have been ascending and are now approaching the upper boundary of the glaciers, indicating accelerated glacier wastage. If the trend since the 1990s continues for the YL and AX glaciers, then the disappearance of these glaciers is inevitable because they are about to lose their accumulation areas; thus, no snow supply is expected for these glaciers. However, all three glaciers show decadal oscillations different from one another but broadly consistent with typical climate signals seen in glaciers worldwide. Rarely in the world are monotonic or steady exponential trends seen in glacier change and ELA records, and these three are no exception to the usual. On the longer time scale of the whole ELA records for the period 1970–2007, all three glaciers show a slight increasing trend (0.8 to 3.4 $\mathrm{m\,yr^{-1}}$) of the ELA, thus projecting a long-term retreat of all three but also slower long-term changes than the trends since the 1990s would suggest.

Spatial Distribution of ELA Trend. It is difficult to assess the spatial representativeness of the observed glacier wastage. To address this problem, we computed the mass balance for the Asian domain (25°–55°N, 60°–110°E; Fig. S6) using the same approaches as those employed above. However, the calculation did not involve downscaling or calibration, meaning that we are unable to discuss the location of the calculated ELAs in terms of the altitudinal extent of existing glaciers in the domain. Consequently, we focus on the trend in ELA during the last two decades (Fig. 3*A*).

In Fig. 3, statistically significant trends are colored. The variability of the calculated ELAs is consistent with that observed, though some biases are found (Fig. S7 and Table S3). If the ELA is located higher than the preferable ELA, as is the case for the three benchmark glaciers (Fig. 2 *A*–*C*), the ascending (descending) ELA results in acceleration (suppression) of glacier wastage. The available observational data reveal negative glacier mass balances and volumetric wastage, suggesting that the recent ELA fluctuates above the elevation of the preferable ELA in the domain (4–6). In Fig. 3, patchy areas of white and pale red in Nepal correspond, respectively, to the stable and acceleration of glacier wastage and are consistent with the observed glacier wastage, as outlined above. In addition, the accelerated wastage of glaciers in southeastern Tibet, as recently observed (23), also supports the ELA trend.

In Nepal, the distribution of the ELA trend appears to be influenced by the trend in summer mean temperature (June–August; Fig. 3*B*) rather than the trend in annual precipitation (Fig. 3*C*). Across the wider Asian domain, however, the warming trend in summer temperature does not always influence the ELA trend. For example, the descending ELA over western Tibet and the ascending ELA over Pamir (at the border between Afghanistan and Tajikistan) appear to reflect changes in annual precipitation (an increase in Tibet and a decrease in Pamir) rather than the trend in the summer mean temperature. In contrast to the occurrence of a dominant warming trend throughout the Asian domain (Fig. 3*B*), the ELA trend is spatially heterogeneous (Fig. 3*A*), probably due to spatial variations in the sensitivity of glacier mass balance to warming, which is strongly affected by the seasonality in precipitation (10). In addition, the ELA shows a significant descending trend for 1976–1995 in the Karakorum and Pamir regions (Fig. S8*A*). It is unknown whether the ELA in these regions was located above or below the preferable ELA during this period; consequently, we are unable to assess whether the glaciers were in a state of mass loss or gain. Nevertheless, this ELA trend supports at least that stable or advancing glaciers could have been driven by cooling and wetting in these regions (Fig. S8 *B* and *C*) (24, 25).

Discussion

We calculated the shrinkage rate of Himalayan glaciers based on in situ measurements. The wastage rates of the glaciers are equivalent to the global mean during the last decade, but are higher than the global mean during the previous two decades (Fig. 1*B*). Two glaciers located in humid environments (and thus at lower altitudes) showed accelerated wastage against a suppressed glacier wastage in an arid environment (and thus at a higher altitude) (Fig. 1*C*). Mass balance calculations indicate that the glacier in an arid environment will survive under the recent climate, whereas the other two glaciers, located in humid environments, are doomed to disappear over time (Fig. 2). It should be noted, however, that some glaciers with accumulation areas located at higher altitudes than those of the recent ELAs will not disappear, even in humid regions. Available in situ data have generally been obtained for glaciers that afford relatively easy

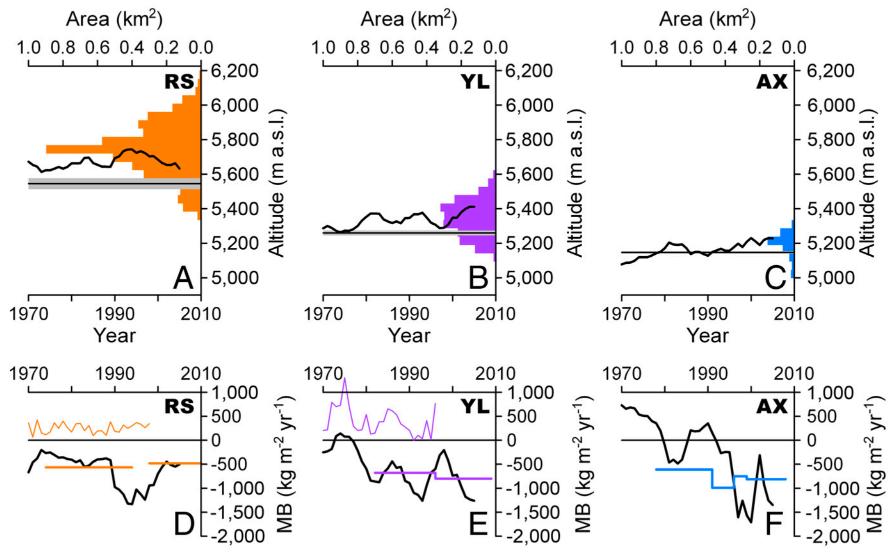

Fig. 2. Area–altitude distribution (color bars), calculated ELA (thick line, five-year running mean), and preferable ELA for the present-day glacier extent (straight line with gray shading) for three benchmark glaciers in Nepal (*Upper*). (*Lower*) The area-averaged mass balance (MB; thick line, five-year running mean), as calculated to yield the minimum rmse against the observation (thick colored line), and the ice core derived mass balances (thin colored lines).

access. Because such glaciers are located at lower altitudes and therefore tend to have higher melt rates, ground-based observational data are probably biased toward a negative mass balance compared with the regional mean under the present-day warming climate. To describe or project changes in ice resources in regional scale, a glacier inventory is required (26), including data on the area–altitude distribution.

The spatial distribution of the ELA trend for the past two decades provides an indication of the spatial representativeness of the observed data. The disappearance of Himalayan glaciers was not only overstated in the Intergovernmental Panel on Climate Change report (2), but also asserted in a study based on analyses of a Himalayan ice core (27). Disappearance may be the fate of some glaciers located at lower altitudes, as indicated by the present results; however, the heterogeneous distribution of the ELA trend suggests that it is unwarranted to draw conclusions regarding the fate of all Himalayan glaciers based on a small number of examples, especially when the benchmark glaciers are chosen in part for their small size, small elevation range, and simple geometry.

Materials and Methods

Surveys of the three benchmark glaciers were performed in the 1990s (14–17) using a theodolite with a laser distance finder. Vertical and horizontal angles were measured from baselines between benchmarks installed around the glaciers (Fig. S5). Between 2008 and 2010, we resurveyed the glaciers using a single frequency carrier-phase differential GPS. One GPS receiver was set on the ground as a base station and the others were used as mobile stations. The locations of benchmarks were measured in static mode and the elevation of the glacier surface was measured in kinematic mode (Fig. S5). All the survey data for the 1990s were superimposed on the same coordinate system (UTM-WGS84) as the GPS surveys to obtain the minimum rmses among the benchmark positions measured in different years (0.81 m in the horizontal and 0.10 m in the vertical). We generated digital elevation models (DEMs) of the GPS surveys (resolution, 10 m) using the inverse distance weighted method; grid cells without GPS measurement points were excluded from subsequent analyses (28). Changes in the surface elevation (elevation change) of the glaciers were obtained as the elevation difference between a point surveyed in the 1990s and the DEM grid cell that included the surveyed point. The elevation changes were averaged, interpolated, or extrapolated in the 50-m altitude band along with the altitude of the ASTER-DEMs (Fig. S4). Finally, the area-average mass balances were obtained from the area-weighted elevation changes multiplied by the density of ice (900 kg m^{-3}) and divided by the observation period.

Approaches for projecting glacier mass balance based on a temperature index, whose relationships are established for glaciers under a Euro-American climate (8, 9), do not necessarily capture the complex responses of monsoon-affected glaciers to climate change (10). Even if calibration is performed with local hydrological data over the Tibetan Plateau (29), the use of a single temperature index would not guarantee an accurate estimate of the glacier response to future warming because a change in surface albedo would alter the temperature index. We therefore use the energy–mass balance model (18) to understand the fluctuations in the glaciers and their fate. The model calculates the daily heat balance at the glacier surface, including

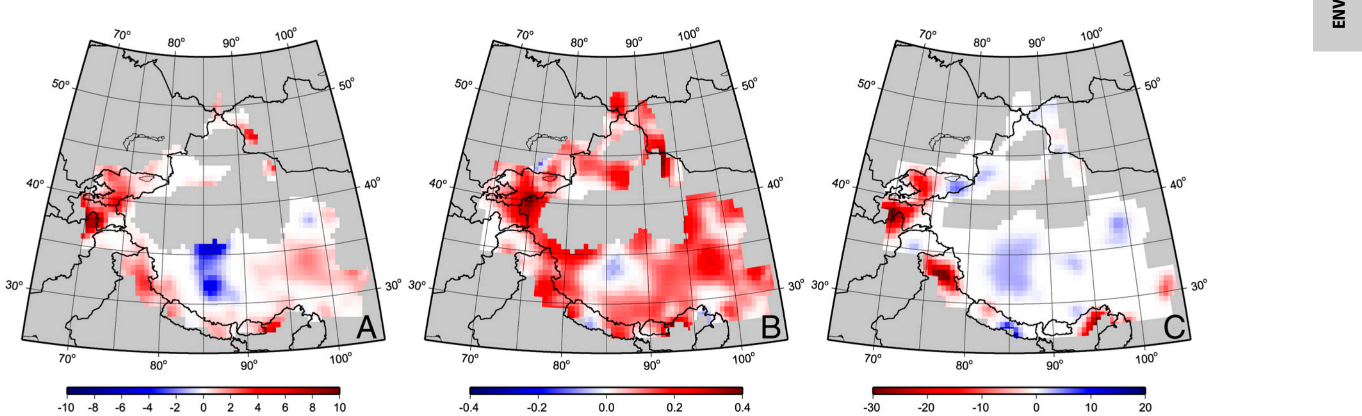

Fig. 3. Spatial distribution of the trends in ELA (*A*), summer mean temperature (*B*), and annual precipitation (*C*) for the period 1988–2007.

the radiation balance, sensible and latent turbulent heat fluxes, heat conduction into the glacier, and mass balance consisting of snow accumulation, melt, refreezing, and evaporation (see *SI Text*). We computed the mass balance at intervals of 50 m in altitude and then obtained the area-averaged mass balance using the area–altitude distribution. We calibrated the temperature offset to obtain the minimum rmse from the observed mass balance at each glacier (Fig. 2). ELA was calculated as the altitude where the mass balance profile crosses zero (kg m^{-2} yr^{-1}). We simultaneously calculated the preferable ELA for each glacier (i.e., the ELA that yields a zero area-averaged mass balance) by uniformly changing the air temperature throughout the calculated period. The amount and seasonality of precipitation affect the mass balance profile (10); consequently, the average and standard deviation of the preferable ELA were obtained for the 37 calculation results (i.e., for the 37 y between 1971 and 2007).

Because long-term climate data are unavailable for the Himalayan region, we used recently archived gridded climate datasets (19, 20) in which daily values of surface air temperature, solar radiation, and precipitation are available at a spatial resolution of $0.5° \times 0.5°$. We downscaled the daily air temperature and precipitation in the datasets by comparison with in situ meteorological observations taken near the glaciers for short periods, yielding statistically significant correlations (see *SI Text* and Table S2).

To obtain the spatial distribution of the ELA trend, air temperature, solar radiation, and precipitation were used from the datasets described above (19, 20). We did not employ downscaling of the input or calibration with the mass balance except for air temperature, for which we reduced the annual variability of the gridded air temperature. We simply calculated the mass balance of each grid cell at altitude intervals of 50 m and then obtained the ELA for each year. We validated calculated ELAs with observed ones (see *SI Text*, and Fig. S7, Table S3). The obtained correlation coefficients (r in Table S3) indicate that the calculation performs well in reproducing the ELA fluctuations in the Asian domain, suggesting that it is valid to at least discuss the temporal trends. For all variables (ELA, summer mean temperature, and annual precipitation), we applied the Mann–Kendall trend test and excluded trends with a probability greater than 5% (Fig. 3 and Fig. S8). Glacierized area and its neighboring area are shown in the figures.

ACKNOWLEDGMENTS. We are deeply indebted to the Department of Hydrology and Meteorology, Nepal, for providing the opportunity to conduct field observations, and to Guide For All Seasons for its long-lasting logistical support during our field surveys. We thank our senior colleagues for their pioneering works in the Himalayas, on which this study stands. We thank S. Takenaka, S. Okamoto, S. Sugiyama, S. Yamaguchi, K. Fukui, R. Nishii, Y. Hoshina, T. Fukuda, and N. S. Pradhananga for their support in field surveys conducted from 2008 to 2010. We acknowledge J. G. Cogley for providing global mean data of glacier mass balance, and J. S. Kargel and an anonymous reviewer for their valuable comments. This study was supported by a Grant-in-Aid for Scientific Research (19253001) from Ministry of Education, Culture, Sports, Science and Technology, Japan.

1. Cogley JG, Kargel JS, Kaser G, van der Veen CJ (2010) Tracking the source of glacier misinformation. *Science* 327:522.
2. Cruz RV, et al. (2007) *Climate Change 2007: Impacts, Adaptation and Vulnerability. Contribution of Working Group II to the Fourth Assessment Report of the Intergovernmental Panel on Climate Change*, eds ML Parry et al. (Cambridge Univ Press, Cambridge, UK), pp 469–506.
3. Raina VK (2009) Himalayan glaciers: A state-of-art review of glacial studies, glacial retreat and climate change. p 60 (discussion paper, Ministry of Environment and Forests, Government of India, New Delhi).
4. Meier MF (1984) Contribution of small glaciers to global sea level. *Science* 226:1418–1421.
5. Kaser G, Cogley JG, Dyurgerov MB, Meier MF, Ohmura A (2006) Mass balance of glaciers and ice caps: Consensus estimates for 1961–2004. *Geophys Res Lett* 33:L19501.
6. Cogley JG (2009) Geodetic and direct mass-balance measurements: Comparison and joint analysis. *Ann Glaciol* 50(50):96–100.
7. Oerlemans J, Fortuin JPF (1992) Sensitivity of glaciers and small ice caps to greenhouse warming. *Science* 258:115–117.
8. Raper SCB, Braithwaite RJ (2006) Low sea level rise projections from mountain glaciers and icecaps under global warming. *Nature* 439:311–313.
9. Radić V, Hock R (2011) Regionally differentiated contribution of mountain glaciers and ice caps to future sea-level rise. *Nat Geosci* 4:91–94.
10. Fujita K (2008) Effect of precipitation seasonality on climatic sensitivity of glacier mass balance. *Earth Planet Sci Lett* 276:14–19.
11. Braithwaite RJ, Raper SCB (2009) Estimating equilibrium-line altitude (ELA) from inventory data. *Ann Glaciol* 50(53):127–132.
12. Pelto MS (2006) The current disequilibrium of North Cascade glaciers. *Hydrol Process* 20:769–779.
13. Wagnon P, et al. (2007) Four years of mass balance on Chhota Shigri Glacier, Himachal Pradesh, India, a new benchmark glacier in the western Himalaya. *J Glaciol* 53:603–611.
14. Fujita K, Kadota T, Rana B, Kayastha RB, Ageta Y (2001) Shrinkage of glacier AX010 in Shorong region, Nepal Himalayas in the 1990s. *Bull Glaciol Res* 18:51–54.
15. Kadota T, Fujita K, Seko K, Kayastha RB, Ageta Y (1997) Monitoring and prediction of shrinkage of a small glacier in the Nepal Himalaya. *Ann Glaciol* 24:90–94.
16. Fujita K, Nakawo M, Fujii Y, Paudyal P (1997) Changes in glaciers in Hidden Valley, Mukut Himal, Nepal Himalayas, from 1974 to 1994. *J Glaciol* 43:583–588.
17. Fujita K, Takeuchi N, Seko K (1998) Glaciological observations of Yala Glacier in Langtang Valley, Nepal Himalayas, 1994 and 1996. *Bull Glacier Res* 16:75–81.
18. Fujita K, Ageta Y (2000) Effect of summer accumulation on glacier mass balance on the Tibetan Plateau revealed by mass-balance model. *J Glaciol* 46:244–252.
19. Hirabayashi Y, Kanae S, Motoya K, Masuda K, Döll P (2008) A 59-year (1948–2006) global near-surface meteorological data set for land surface models. Part I: Development of daily forcing and assessment of precipitation intensity. *Hydrol Res Lett* 2:36–40.
20. Yatagai A, et al. (2009) A 44-year daily gridded precipitation dataset for Asia based on a dense network of rain gauges. *SOLA* 5:137–140.
21. Fujita K, et al. (2006) Thirty-year history of glacier melting in the Nepal Himalayas. *J Geophys Res* 111:D03109.
22. Takeuchi N, et al. (2009) A snow algal community on the surface and in an ice core of Rikha-Samba Glacier in Western Nepali Himalayas. *Bull Glaciol Res* 27:25–35.
23. Yang W, et al. (2010) Characteristics of recent temperate glacier fluctuations in the Parlung Zangbo River basin, southeast Tibetan Plateau. *Chinese Sci Bull* 55:2097–2102.
24. Hewitt K (2005) The Karakoram anomaly? Glacier expansion and the 'elevation effect', Karakoram Himalaya. *Mt Res Dev* 25:332–340.
25. Scherler D, Bookhagen B, Strecker MR (2011) Spatially variable response of Himalayan glaciers to climate change affected by debris cover. *Nat Geosci* 4:156–159.
26. Ohmura A (2009) Completing the world glacier inventory. *Ann Glaciol* 50(53):144–148.
27. Kehrwald NM, et al. (2008) Mass loss on Himalayan glacier endangers water resources. *Geophys Res Lett* 35:L22503.
28. Fujita K, Suzuki R, Nuimura T, Sakai A (2008) Performance of ASTER and SRTM DEMs, and their potential for assessing glacial lakes in the Lunana region, Bhutan Himalaya. *J Glaciol* 54:220–228.
29. Immerzeel WW, van Beek LPH, Bierkens MFP (2010) Climate change will affect the Asian water towers. *Science* 328:1382–1385.

Supporting Information

Fujita and Nuimura 10.1073/pnas.1106242108

SI Text

Observations on Three Benchmark Glaciers. Observations on the three benchmark glaciers in the Nepal Himalayas were started in the 1970s (Table S1). The termini of all three glaciers have been in retreat since this time (Figs S1–S3).

Area-Altitude Distribution of Glaciers. The present calculations require the area–altitude distribution of each glacier to obtain the area-averaged mass balance. We used recent satellite images of ASTER and digital elevation models (DEMs) derived from ASTER data to delineate the boundaries of glaciers and to obtain the area–altitude distribution (Table S1; Fig. 2 and Fig. S4). The altitude and horizontal shift of DEMs in each region were calibrated to yield the minimum rms error (rmse) from the global positioning system (GPS) data on glacier-free terrain (1). The rmses range from 8.5 to 11.8 m.

Digitizing a 1982 Topographical Map of the Yala Glacier. A topographical map of the Yala Glacier was produced in 1982 by ground photogrammetry (2). We digitized the contour lines (10-m interval) on this map and converted the line data to a 10-m-resolution DEM using the ANUDEM algorithm in the software ArcGIS 9.2. The accuracy of the DEM was validated in the same manner as that described above, yielding a rmse of 12.6 m. This DEM was used to revise the previously calculated mass balance of the Yala Glacier between 1982 and 1996 (3).

Changes in Glacier Surface Elevation Derived from Geodetic Surveys. Surveys of the three benchmark glaciers were performed in the 1990s (3–6) using a theodolite with a laser distance finder (Total Station SET2100, Sokkia). Vertical and horizontal angles were measured from baselines between benchmarks installed around the glaciers (Fig. S5). Between 2008 and 2010, we resurveyed the glaciers using a single frequency carrier-phase differential GPS (Pro Mark 3, Magellan). One GPS receiver was set on the ground as a base station, and the others were used as mobile stations. The locations of benchmarks were measured in static mode and the elevation of the glacier surface was measured in kinematic mode (Fig. S5). All the measured data were postprocessed using Global Navigation Satellite Systems Solutions software (Ashtech). GPS data with accuracy worse than 1 m in both the horizontal and vertical were excluded from subsequent analyses. All the survey data for the 1990s were superimposed on the same coordinate system (UTM-WGS84) as the GPS surveys to obtain the minimum rmses among the benchmark positions measured in different years (0.81 m in the horizontal and 0.10 m in the vertical) (1). We generated DEMs of the GPS surveys (resolution, 10 m) using the inverse distance weighted method; grid cells without GPS measurement points were excluded from subsequent analyses. Changes in the surface elevation (elevation change) of the glaciers were obtained as the elevation difference between a point surveyed in the 1990s and the DEM grid cell that included the surveyed point. The elevation changes were averaged, interpolated, or extrapolated in the 50-m altitude band along with the altitude of the ASTER-DEMs (Fig. S4). Finally, the area–average mass balances were obtained from the area-weighted elevation changes multiplied by the density of ice (900 $\mathrm{kg\,m^{-3}}$) and divided by the observation period.

Uncertainty Analysis of Geodetic Surveys. The accuracy of area-averaged mass balance derived from geodetic surveys (σ) was evaluated as follows:

$$\sigma = \left(\sum A_z(\sigma_s + \sigma_k + \sigma_p) + \sum dA_z|h_z| + \sum A_z|h_z|\sigma_d\right) / \sum A_z, \qquad \textbf{[S1]}$$

where A_z and $|h_z|$ denote the area and absolute value of elevation change in the 50-m altitude band. The error in the elevation change (σ_s) corresponds to variability (the standard deviation) in the elevation change within the 50-m altitude band. The value of the uppermost band is used at unmeasured higher altitudes. The accuracy of kinematic GPS measurements (σ_k) is obtained as the average of the height accuracy, which is generated in the postprocessing of GPS data for each glacier (0.21–0.23 m). The error related to the superimposition of two surveys (σ_p) is evaluated as the averaged rmse of benchmark positions around the glaciers (0.1 m). The accuracy of delineating the glacier boundary (dA_z) is assumed to be half a pixel in the ASTER-VNIR image (7.5 m) multiplied by the boundary length of each 50-m altitude band. The uncertainty in the density of ice (σ_d) is assumed to be 30 $\mathrm{kg\,m^{-3}}$. Finally, we obtained the uncertainty of the area-averaged mass balance for each glacier (σ), yielding values ranging from 50 to 85 $\mathrm{kg\,m^{-2}\,yr^{-1}}$ (Fig. 1).

Energy–Mass Balance Model. Approaches based on a temperature index, whose relationships are established for glaciers under a Euro-American climate (7, 8), do not necessarily capture the complex responses of monsoon-affected glaciers to climate change (9). Even if calibration is performed with local hydrological data (10), the use of a single temperature index would not guarantee an accurate estimate of the glacier response to future warming because a change in surface albedo would alter the temperature index. We therefore performed energy–mass balance calculations for each glacier to understand the fluctuations in the glaciers and their fate. The energy–mass balance model used in this study calculates the daily heat balance at the glacier surface, including the radiation balance, sensible and latent turbulent heat fluxes, heat conduction into the glacier, and mass balance consisting of snow accumulation, melt, refreezing, and evaporation, as follows (11, 12):

$$\max[Q_M;0] = (1-\alpha)R_S + R_L - \min[\sigma T_S^4; 315.6] + Q_S + E_V l_e + Q_G. \qquad \textbf{[S2]}$$

Heat for melting (Q_M) is obtained if the right-hand side of the equation is greater than zero. Absorbed short-wave radiation is calculated from the surface albedo (α) and downward short-wave radiation (R_S). Downward long-wave radiation (R_L) is calculated from air temperature, relative humidity, and the ratio of downward short-wave radiation at the top of the atmosphere, using an empirical scheme (11). Upward long-wave radiation is obtained from the Stefan–Boltzmann constant (σ) and the surface temperature in Kelvin (T_S), assuming a black body for the snow/ice surface. A melting surface (0 °C surface temperature) releases upward long-wave radiation of 315.6 ($\mathrm{W\,m^{-2}}$). Sensible (Q_S) and latent ($E_V l_e$) turbulent heat fluxes are obtained by bulk methods. The latent heat for evaporation of water or ice (l_e) is determined from the surface temperature. Conductive heat into the glacier ice (Q_G) is obtained by calculating the temperature profile of the snow layer and/or glacier ice. All heat components are positive when fluxes are directed toward the surface. The mass balance (B) at any location on the glacier is calculated as follows:

$$B = Ca - Q_M/l_m + E_V + R_F. \quad \text{[S3]}$$

Solid precipitation (Ca, positive sign), which is determined along with air temperature, is equivalent to accumulation over the glacier. Mass is removed from the glacier as meltwater (Q_M/l_m, positive sign) and evaporation (E_V, negative sign). l_m is the latent heat for melting ice. Some of the meltwater is fixed to the glacier by refreezing (R_F, positive sign) if the glacier ice is cold enough (13). The refreezing amount is calculated in the model by considering the conduction of heat into glacier ice and the presence of water at the interface between the snow layer and glacier ice (11). Also considered is refreezing during winter and during shorter cooling events. Special attention is paid to the treatment of the surface albedo (α) because it varies enormously in space and time, even for a single glacier (the albedo declines down the glacier and during the course of the melt season). The albedo in the model was calculated according to the surface snow density, which changes with snow compaction. The albedo of bare ice was set to 0.2. Detailed schemes for the entire model have been described previously (11, 12, 14).

Downscaling Input Climate Data. Because long-term climate data are unavailable for the Himalayan region, we used recently archived gridded climate datasets (15, 16) in which daily values of surface air temperature, solar radiation, and precipitation are available at a spatial resolution of 0.5° × 0.5°. We downscaled the daily air temperature and precipitation in the datasets by comparison with in situ meteorological observations taken near the glaciers for short periods (3, 17, 18), yielding statistically significant correlations (Table S2). The slopes of linear regression for the air temperature (a_{AT}) range from 0.51 to 0.58, indicating that the seasonal variability in gridded air temperature is about twice the variability measured in situ. The slopes of the linear regression for precipitation (a_{PR}) suggest that the gridded precipitation is overestimated for the Rikha Samba Glacier ($a_{PR} < 1$) and underestimated for the Yala Glacier and for Glacier AX010 ($a_{PR} > 1$). The Rikha Samba Glacier is located north of the Annapurna massif, which records the maximum precipitation in Nepal. The gridded precipitation is based on the instrumental record from near the Annapurna massif, whereas the Rikha Samba Glacier is affected by the relatively arid Tibetan climate. Precipitation over the other two glaciers appears to be influenced by orographic effects (i.e., greater precipitation in areas of higher altitude). The annual precipitation data in Fig. 1*C* are the average values of these linear regressions. This type of calibration is required for precise calculations of the mass balance of individual glaciers. Relative humidity data are from the National Centers for Environmental Prediction/National Center for Atmospheric Research (NCEP/NCAR) reanalysis dataset (a spatial resolution of 2.5° × 2.5°) (19) without downscaling. The lapse rate of air temperature is an important factor in calculating an altitudinal profile of the mass balance. We prepared the daily lapse rate in grids that included the individual glaciers, using the air temperatures and geopotential heights at 400 and 500 hPa in the NCEP/NCAR reanalysis dataset (19). Because wind speed has little influence on the mass balance results (11), it was assumed to be constant ($4.0\ \mathrm{m\,s^{-1}}$).

Mass Balance Calculations. We computed the mass balance at intervals of 50 m in altitude and computed the area-averaged mass balance using the area–altitude distribution obtained above. We calibrated the temperature offset to obtain the minimum rmse from the observed mass balance at each glacier (Fig. 2). Fig. 2 also shows mass balances reconstructed from analyses of ice cores recovered from the Rikha Samba (RS) and Yala (YL) glaciers (20, 21). For the RS glacier, an insignificant correlation ($r = -0.30$) is obtained between the calculated mass balance and that derived from the ice core, because the core was obtained at such a high altitude [5,880 m a.s.l. (above sea level)] that the reconstructed mass balance represents accumulation (21). In contrast, a significant correlation is obtained for the YL glacier ($r = 0.69$, $p < 0.001$) because the YL ice-core record, which was reconstructed for an altitude of 5,380 m a.s.l., was influenced by significant melt and thus corresponds to the area-averaged mass balance (20).

Equilibrium-line altitude (ELA) was calculated as the altitude where the mass balance profile crosses zero ($\mathrm{kg\ m^{-2}\,y^{-1}}$). We simultaneously calculated the preferable ELA for each glacier (i.e., the ELA that yields a zero area-averaged mass balance) by uniformly changing the air temperature throughout the calculated period. The amount and seasonality of precipitation affect the mass balance profile (9); consequently, the average and standard deviation of the preferable ELA were obtained for the 37 calculation results (i.e., for the 37 years between 1971 and 2007).

ELA Trends. To obtain the spatial distribution of the ELA trend, we did not employ downscaling of the input or calibration with the mass balance except for air temperature. Air temperature, solar radiation, and precipitation were used from the datasets described above (15, 16). The long-term mean (37 years from 1971 to 2007) of daily relative humidity at the surface and the daily lapse rate between 400 and 500 hPa were calculated using the NCEP/NCAR reanalysis dataset (19). Wind speed was assumed to be constant ($4.0\ \mathrm{m\,s^{-1}}$). Annual variability of the gridded air temperature is twice larger than the observed one (Table S2) and affects the sensitivity of glacier mass balance to climate change (8). We reduced the annual variability of the gridded air temperature as

$$T_c = 0.5(T_g - \overline{T_g}) + \overline{T_g}, \quad \text{[S4]}$$

where T_c and T_g denote the calibrated and gridded daily air temperature. Annual variability of air temperature from the annual average ($\overline{T_g}$) was decreased by half.

We simply calculated the mass balance of each grid cell at altitude intervals of 50 m and then obtained the ELA for each year. Although significant offsets were found among the observed (22–26) and calculated ELAs (dELA in Table S3), the temporal changes in anomalies from individual averages show good consistency with each other, except for the Kara-Batkak and Urumqi No. 1 glaciers (Fig. S7; Table S3). The inconsistencies are presumably due to the quality of the original gridded dataset, because we were able to accurately reproduce the Kara-Batkak ELA when calibrating another gridded climate dataset with the in situ observational data at a neighboring glacier (27) (orange line in Fig. S7,). The obtained correlation coefficients (r in Table S3) indicate that the calculation performs well in reproducing the ELA fluctuations in the Asian domain, suggesting that it is valid to at least discuss the temporal trends. For all variables (ELA, summer mean temperature, and annual precipitation), we applied the Mann–Kendall trend test and excluded trends with a probability greater than 5% (Fig. 3 and Fig. S8). Glacierized area and its neighboring area are shown in the figures.

1. Fujita K, Suzuki R, Nuimura T, Sakai A (2008) Performance of ASTER and SRTM DEMs, and their potential for assessing glacial lakes in the Lunana region, Bhutan Himalaya. *J Glaciol* 54:220–228.
2. Yokoyama K (1984) Ground photogrammetry of Yala Glacier, Langtang Himal, Nepal Himalaya. *Report of the Boring Project 1981–82 in the Nepal Himalaya, Data Cent for Glacier Res, Jpn Soc of Snow and Ice*, Tokyo, Publ 2:99–105.
3. Fujita K, Takeuchi N, Seko K (1998) Glaciological observations of Yala Glacier in Langtang Valley, Nepal Himalayas, 1994 and 1996. *Bull Glacier Res* 16:75–81.
4. Fujita K, Kadota T, Rana B, Kayastha RB, Ageta Y (2001) Shrinkage of Glacier AX010 in Shorong region, Nepal Himalayas in the 1990s. *Bull Glaciol Res* 18:51–4.
5. Kadota T, Fujita K, Seko K, Kayastha RB, Ageta Y (1997) Monitoring and prediction of shrinkage of a small glacier in the Nepal Himalaya. *Ann Glaciol* 24:90–94.

6. Fujita K, Nakawo M, Fujii Y, Paudyal P (1997) Changes in glaciers in Hidden Valley, Mukut Himal, Nepal Himalayas, from 1974 to 1994. *J Glaciol* 43:583–588.
7. Raper SCB, Braithwaite RJ (2006) Low sea level rise projections from mountain glaciers and icecaps under global warming. *Nature* 439:311–313.
8. Radić V, Hock R (2011) Regionally differentiated contribution of mountain glaciers and ice caps to future sea-level rise. *Nat Geosci* 4:91–94.
9. Fujita K (2008) Effect of precipitation seasonality on climatic sensitivity of glacier mass balance. *Earth Planet Sci Lett* 276:14–19.
10. Immerzeel WW, van Beek LPH, Bierkens MFP (2010) Climate change will affect the Asian water towers. *Science* 328:1382–1385.
11. Fujita K, Ageta Y (2000) Effect of summer accumulation on glacier mass balance on the Tibetan Plateau revealed by mass-balance model. *J Glaciol* 46:244–252.
12. Fujita K, Ohta T, Ageta Y (2007) Characteristics and climatic sensitivities of runoff from a cold-type glacier on the Tibetan Plateau. *Hydrol Process* 21:2882–2891.
13. Fujita K, Seko K, Ageta Y, Pu J, Yao T (1996) Superimposed ice in glacier mass balance on the Tibetan Plateau. *J Glaciol* 42:454–460.
14. Fujita K (2007) Effect of dust event timing on glacier runoff: Sensitivity analysis for a Tibetan glacier. *Hydrol Process* 21:2892–2896.
15. Hirabayashi Y, Kanae S, Motoya K, Masuda K, Döll P (2008) A 59-year (1948–2006) global near-surface meteorological data set for land surface models. Part I: Development of daily forcing and assessment of precipitation intensity. *Hydrol Res Lett* 2:36–40.
16. Yatagai A, et al. (2009) A 44-year daily gridded precipitation dataset for Asia based on a dense network of rain gauges. *SOLA* 5:137–140.
17. Fujita K, Sakai A, Chhetri TB (1997) Meteorological observation in Langtang Valley, 1996. *Bull Glacier Res* 15:71–78.
18. Fujita K, Nakazawa F, Rana B (2001) Glaciological observations on Rikha Samba Glacier in Hidden Valley, Nepal Himalayas, 1998 and 1999. *Bull Glaciol Res* 18:31–35.
19. Kalnay E, et al. (1996) The NCEP/NCAR 40-year reanalysis project. *Bull Amer Meteorol Soc* 77:437–471.
20. Fujita K, et al. (2006) Thirty-year history of glacier melting in the Nepal Himalayas. *J Geophys Res* 111:D03109.
21. Takeuchi N, et al. (2009) A snow algal community on the surface and in an ice core of Rikha-Samba Glacier in Western Nepali Himalayas. *Bull Glaciol Res* 27:25–35.
22. Dyurgerov MB (2002) *Glacier mass balance and regime: Data of measurements and analysis*. Occasional Paper 55 (Institute of Arctic and Alpine Research, Univiversity of Colorado, Boulder, CO).
23. WGMS (2005) *Fluctuations of Glaciers 1995-2000*, eds Haeberli W, et al. (World Glacier Monitoring Service, Zurich, Switzerland), Vol VIII.
24. WGMS (2008) *Fluctuations of Glaciers 2000-2005*, eds Haeberli W, et al. (World Glacier Monitoring Service, Zurich, Switzerland), Vol IX.
25. Fujita K, Ageta Y, Pu J, Yao T (2000) Mass balance of Xiao Dongkemadi Glacier on the central Tibetan Plateau from 1989 to 1995. *Ann Glaciol* 31:159–163.
26. Pu J, et al. (2008) Rapid decrease of mass balance observed in the Xiao (Lesser) Dongkemadi Glacier, in the central Tibetan Plateau. *Hydrol Process* 22:2953–2958.
27. Fujita K, et al. (2011) Favorable climatic regime for maintaining the present-day geometry of the Gregoriev Glacier, Inner Tien Shan. *The Cryosphere* 5:539–549.

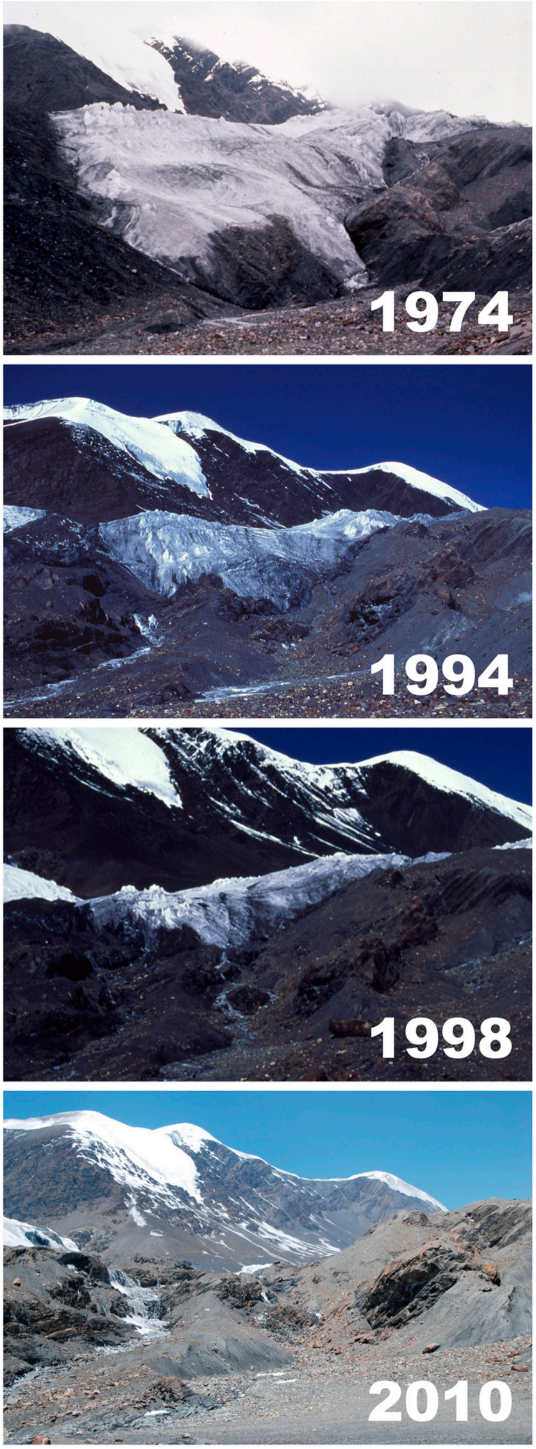

Fig. S1. Photographs of the terminus of Rikha Samba Glacier between 1974 and 2010. Photographs were taken by Y. Fujii (1974) and K. Fujita (1994, 1998, and 2010).

Fig. S2. Photographs of the terminus of Yala Glacier between 1982 and 2009. Photographs were taken by S. Kohshima (1982) and K. Fujita (1996, 2008, and 2009).

Fig. S3. Photographs of the terminus of Glacier AX010 between 1978 and 2008. Photographs were taken by Y. Ageta (1978), T. Kadota (1989), and K. Fujita (1998 and 2008).

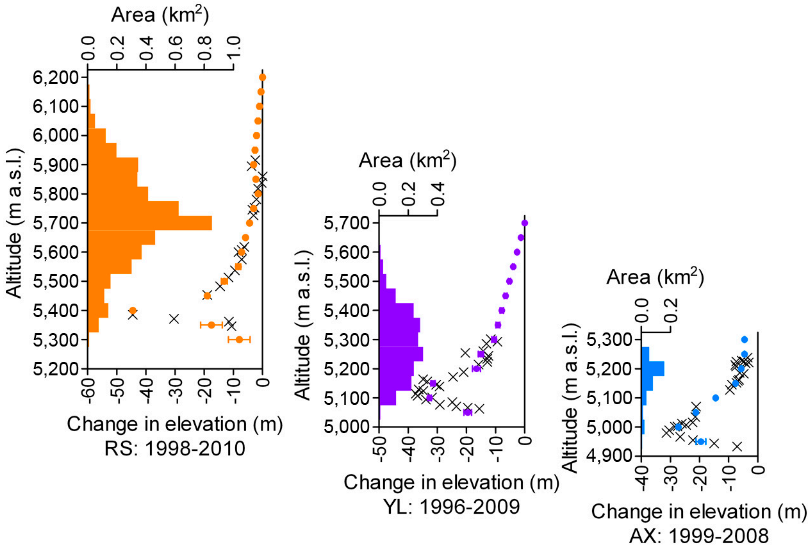

Fig. S4. Altitudinal profiles of the surface area (colored bars, 50-m interval) and elevation change for the Rikha Samba Glacier (RS), Yala Glacier (YL), and Glacier AX010 (AX). Crosses denote observed elevation changes. Colored circles denote and interpolated/extrapolated at 50-m interval.

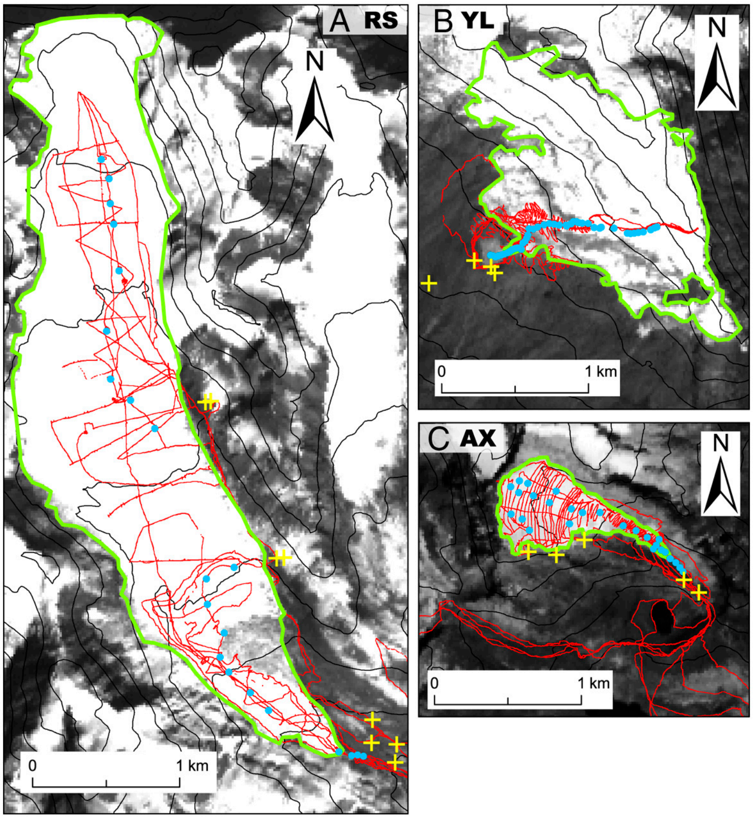

Fig. S5. Survey paths on the Rikha Samba Glacier (*A*; RS) Yala Glacier (*B*; YL), and Glacier AX010 (*C*; AX) in the Nepal Himalaya. Light green lines, yellow crosses, light blue circles, and red points denote the glacier boundary, benchmarks, points surveyed in the 1990s, and GPS measurement points of the present study, respectively. Background images are ASTER-VNIR band 1. Contour lines (interval, 100 m) are taken from an ASTER-DEM.

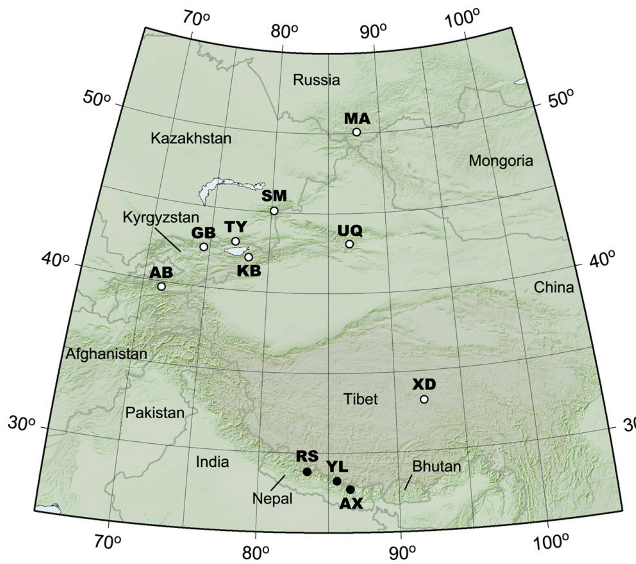

Fig. S6. Locations of three benchmark glaciers in the Nepal Himalayas (solid circles) and glaciers whose mass balance has been measured in situ for more than 10 years (open circles). Equilibrium-line altitude calculations were validated using observed data (Fig. S7; Table S3). Maliy Aktru, MA; Abramov, AB; Shumskiy, SM; Ts. Tuyuksuyskiy, TY; Kara-Batkak, KB; Golubina, GB; Urumqi No. 1, UQ; Xiao Dongkemadi, XD.

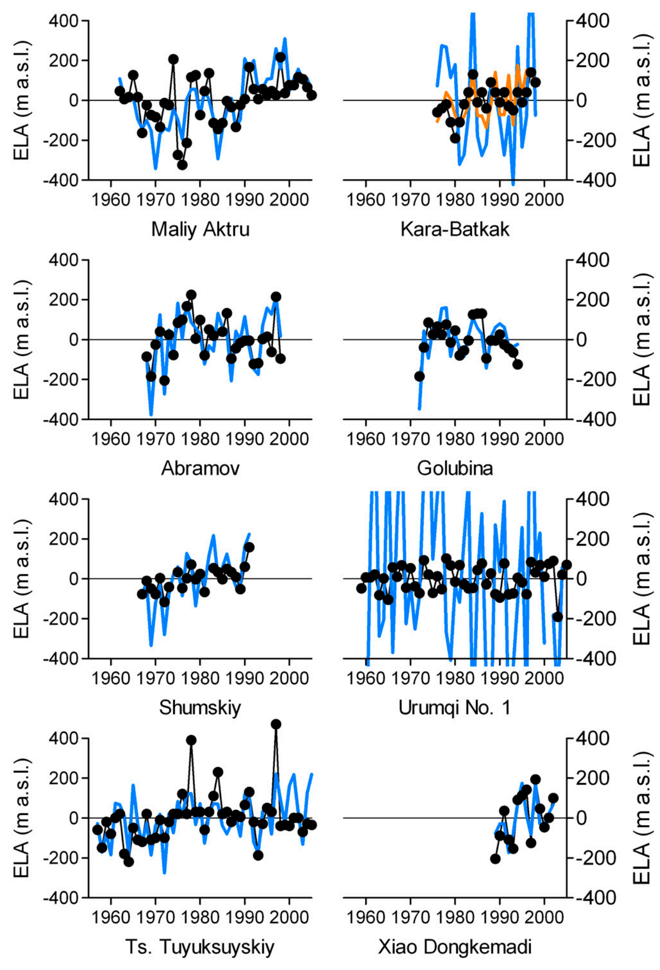

Fig. S7. Anomalies of observed (circles) and calculated (blue lines) equilibrium-line altitudes (ELAs) for Asian glaciers (Fig. S6; Table S3). Some of the calculated ELA anomalies for the Kara-Batkak and Urumqi No. 1 Glaciers are plotted outside of the vertical axis. We were able to accurately reproduce the Kara-Batkak ELA when another gridded climate dataset was calibrated with the in situ observational data at a neighboring glacier (27) (orange line).

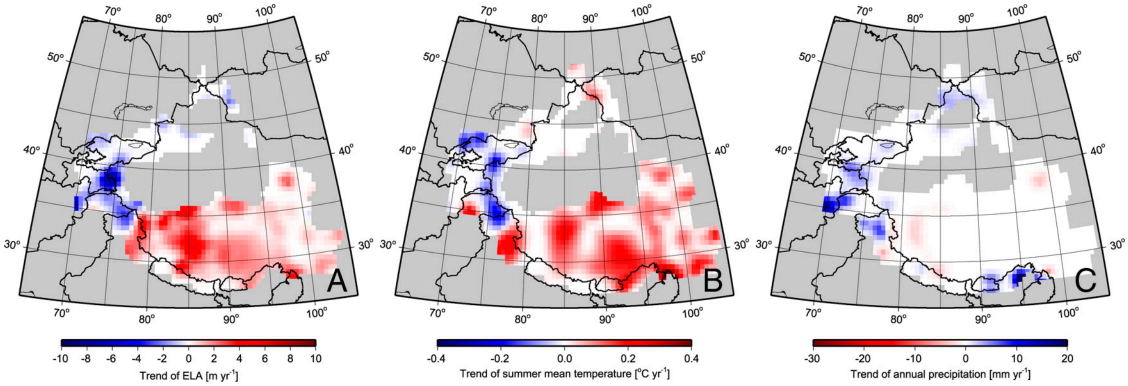

Fig. S8. Spatial distributions of the trend in ELA (*A*), summer mean temperature (*B*), and annual precipitation (*C*) for the period 1976–1995.

Table S1. Geographical locations, observed area-averaged mass balances, and ideal ELA for three benchmark glaciers in Nepal

Glacier	RS	YL	AX
Latitude, °N	28.824	28.237	27.716
Longitude, °E	83.491	85.618	86.556
Lowermost altitude, m a.s.l.	5,346	5,086	4,968
Uppermost altitude, m a.s.l.	6,229	5,642	5,302
Area, km^2	4.62	1.88	0.38
Acquisition date of ASTER data	Dec. 2007	Oct. 2003	Nov. 2004
Area-averaged mass balance for the last decade, kg m^{-2} y^{-1}	−479	−800	−810
Period	1998–2010	1996–2009	1999–2008
Area-averaged mass balance for the 1970s–1990s, kg m^{-2} y^{-1}	−566	−679	−722*
Period	1974–1994	1982–1996	1978–1999
Estimated long-term annual precipitation, mm	374	772	1,611
Preferable ELA, m a.s.l.	5,545	5,260	5,147

*Annual weighted average. RS, YL, and AX denote the Rikha Samba Glacier, Yala Glacier, and Glacier AX010, respectively

Table S2. Parameters used for statistical downscaling of gridded air temperature (AT) and precipitation (PR)

Glacier	RS	YL	AX
a_{AT}	0.538	0.510	0.579
r_{AT}	0.692	0.717	0.793
a_{PR}	0.345	1.113	1.325
r_{PR}	0.535	0.673	0.678

Here we establish a linear regression ($y = ax + b$) between the observed (y) and gridded (x) variables.

r denotes the correlation coefficient between gridded and observed parameters. All significance levels are $p < 0.001$. The intercept of precipitation (b_{PR}) is fixed to zero, to avoid constant precipitation and negative values. RS, YL, and AX denote the Rikha Samba Glacier, Yala Glacier, and Glacier AX010, respectively.

Table S3. Validation of calculated ELAs using observed data (22–26) (Figs S6 and S7)

Glacier	Area and country	Longitude, °E	Latitude, °N	Period, y	dELA, m a.s.l.	r	Missing data
Maliy Aktru, MA	Altai, Russia	87.750	50.083	1962–2005 (44)	534	0.620*	
Abramov, AB	Pamir, Kyrgyzstan	71.500	39.667	1968–1998 (30)	−493	0.767*	1984
Shumskiy, SM	Dzhungariya, Kazakhstan	80.233	45.083	1967–1991 (23)	−303	0.805*	1974, 1982
Ts. Tuyuksuyskiy, TY	Tien Shan, Kazakhstan	77.100	43.000	1957–2005 (49)	48	0.549*	
Kara-Batkak, KB	Tien Shan, Kyrgyzstan	78.300	42.100	1976–1998 (23)	289	0.350(0.569†)	
Golubina, GB	Tien Shan, Kyrgyzstan	74.500	42.450	1972–1994 (23)	40	0.661*	
Urumqi No. 1, UQ	East Tien Shan, China	86.817	43.083	1959–2005 (47)	297	0.285‡	
Xiao Dongkemadi, XD	Central Tibet, China	92.133	33.167	1989–2002 (14)	837	0.821*	

dELA and r denote the difference in averages (calculation minus observation) and the correlation coefficient between calculated and observed ELAs. If the gridded air temperature and precipitation are calibrated with observational data (27), the correlation coefficient for Kara-Batkak Glacier is improved (0.569).

*$p < 0.001$.

†$p < 0.01$.

‡$p < 0.1$.